

# Microscopic theory of the $\gamma$ decay of giant resonances in superfluid nuclei

W.-L. Lv

*Frontiers Science Center for Rare isotopes, Lanzhou University, Lanzhou 730000, China and  
School of Nuclear Science and Technology, Lanzhou University, Lanzhou 730000, China*

Y.-F. Niu\*

*School of Physics and Astronomy, Shanghai Jiao Tong University,  
Key Laboratory for Particle Astrophysics and Cosmology (MoE), Shanghai 200240, China  
Shanghai Key Laboratory for Particle Physics and Cosmology, Shanghai 200240, China  
Frontiers Science Center for Rare isotopes, Lanzhou University, Lanzhou 730000, China and  
School of Nuclear Science and Technology, Lanzhou University, Lanzhou 730000, China*

G. Colò

*Dipartimento di Fisica, Università degli Studi di Milano, via Celoria 16, I-20133 Milano, Italy and  
INFN, Sezione di Milano, via Celoria 16, I-20133 Milano, Italy*

(Dated: March 31, 2026)

Recent advances in experiments have enabled the measurement of  $\gamma$ -decay from giant and pygmy resonances to low-lying states, establishing this technique as a unique probe for nuclear structure. However, a microscopic description of  $\gamma$ -decay to low-lying states in superfluid nuclei is still lacking. We develop the Skyrme quasiparticle vibration (QPVC) model to calculate  $\gamma$ -decay widths between vibrational states. This model treats initial and final states as quasiparticle random phase approximation (QRPA) phonons and includes all the second-order diagrams for the interaction between the quasiparticles and the phonons, while consistently accounting for the polarization processes. The same Skyrme functional is employed for the ground state and the interaction vertices. As a timely application, the  $\gamma$ -decay width from the giant dipole resonance to the  $2_1^+$  state in  $^{140}\text{Ce}$  is calculated, which has recently been measured at the high intensity  $\gamma$ -ray source (HI $\gamma$ S). For the 4 Skyrme functionals we used, the total width of the collective dipole states in GDR region is 200–420 eV and the corresponding branching ratio is 0.75–1.20%. The polarization effect, extracted microscopically, agrees in trend with the macroscopic Bohr-Mottelson formula.

## I. INTRODUCTION

Nuclear electromagnetic transitions serve as a fundamental probe of nuclear structure, offering crucial insights into the properties of excited states and the underlying many-body dynamics [1]. For decades, they have played a central role in advancing the understanding of the nucleus, from revealing nuclear collective motion [2], deformation [3, 4], and new magic numbers [5]. The emission of high-energy  $\gamma$  rays [6] serves as a damping mechanism for nuclear vibration modes [7], including pygmy and giant resonances. Although the  $\gamma$  decay contributes by a tiny fraction to the total damping, compared with spreading width and direct particle emission, it is particularly valuable because the electromagnetic interaction is well understood. Precise  $\gamma$ -decay measurements therefore provide a clean probe of the underlying wave function [8–11].

The branching ratios of  $\gamma$  decay to low-lying states are typically very small, making such decays historically difficult to detect. Recent experimental advances have begun to overcome these challenges. Nuclear resonance fluorescence (NRF) experiments using the High Intensity  $\gamma$ -ray Source (HI $\gamma$ S) [12] enable detailed studies of  $\gamma$  decays from dipole resonances to the  $2_1^+$  state. In Ref. [13], the authors measured the  $\gamma$  decay from the isovector giant dipole resonance (IVGDR) to the  $2_1^+$  state in  $^{154}\text{Sm}$ . By comparing the measured branching ratio  $\sigma_{2_1^+}/\sigma_{\text{ES}}$  with macroscopic geometrical model predictions, they successfully extracted nuclear deformation parameters. In Ref. [14], a similar measurement for the pygmy dipole resonance (PDR) to the  $2_1^+$  state in  $^{150}\text{Nd}$  revealed a significant deviation from the Porter-Thomas distribution, suggesting that the  $\gamma$ SF used in statistical models [15] may require revision. These findings demonstrate that high-energy  $\gamma$  decays from excited resonances to low-lying states are a sensitive probe of nuclear structure and play an important role in refining nuclear astrophysics inputs. More measurements will be carried out at the Laboratori Nazionali di Legnaro (LNL) [16] and Shanghai Synchrotron Radiation Facility (SSRF) [17].

Theoretically, the transition between two excited states requires a careful treatment of the dynamic correlations. Several models based on phenomenological inputs have been employed so far, including the nuclear field theory (NFT) [18, 19], extended

---

\* niuyf@sju.edu.cn

theory of finite Fermi systems (ETFFS) [20], and the quasiparticle phonon model (QPM) [21, 22]. In recent years, the fully self-consistent treatment of  $\gamma$  decay of GRs with the Skyrme particle vibration coupling (PVC) model has become available [23, 24]. In this model the dynamic correlations are considered through the PVC, which has been found important for the single-particle levels [25–28], the Gamow-Teller response and the related  $\beta$  decay [29–34], as well as the spreading widths and centroid energies of giant resonances [35–39]. However, pairing correlations have never been included in the study of the  $\gamma$  decay from GRs to low-lying states with the (Q)PVC model.

In this work, we extend this fully self-consistent approach to superfluid systems by the Skyrme QPVC model. The model incorporates pairing correlations based on Skyrme energy density functionals and is formulated to describe  $\gamma$  decays between vibrational states within the NFT framework. Motivated by recent experiments at the HI $\gamma$ S [40], we employ our model to investigate the  $\gamma$  decay of IVGDR to the  $2_1^+$  state in  $^{140}\text{Ce}$ . This paper is organized as follows. In Sec. II, we present our theoretical formalism. Section III provides the numerical details of the calculation. Our results for  $^{140}\text{Ce}$  are presented and discussed in Sec. IV. We conclude with a summary in Sec. V.

## II. FORMALISM

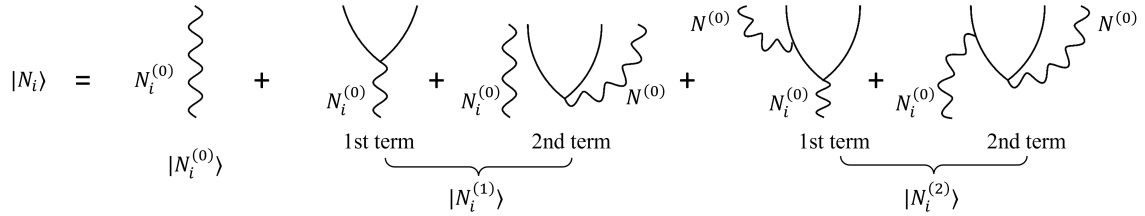


FIG. 1. Perturbation expansion of the wave function  $|N_i\rangle$ . The wavy and solid lines represent the phonon and quasiparticle, respectively. Quasiparticle states are not explicitly labeled due to the possible different contractions among them, as discussed in Appendix B.

We start from the Hamiltonian which describes a system that consists of interacting fermions and bosons [41, 42]

$$H = H_F + H_B + V, \quad (1)$$

where  $H_F$  is the Hamiltonian of single-quasiparticle states ( $|a\rangle$ ) with energy  $E_a$ , and  $H_B$  is the Hamiltonian of QRPA phonons ( $|N^{(0)}\rangle$ ) with energy  $\Omega_N$ , i.e., nuclear vibrations. These two degrees of freedom are coupled through the interaction  $V$ . Here  $V$  includes both the particle-hole (ph) channel of the Skyrme interaction and the particle-particle (pp) channel of the pairing interaction.

For the  $\gamma$  decay between two vibrational states  $|N_i\rangle$  and  $|N_f\rangle$ , we have to consider the interplay between nuclear collective motion and individual particles. In other words, the collective mode dynamically modifies the nuclear mean field in which the particles move. To consider this effect, we work in a fixed quasiparticle basis and treat the interaction  $V$  as a perturbation. The interaction dresses the QRPA phonons by admixing the configurations, such as 2qp and 2qp $\otimes$ phonon, to the QRPA states  $|N^{(0)}\rangle$ . Accordingly, we expand the dressed states as

$$|N\rangle = |N^{(0)}\rangle + |N^{(1)}\rangle + |N^{(2)}\rangle + \dots, \quad (2)$$

where  $|N^{(k)}\rangle$  denotes the  $k$ -th order correction induced by  $V$ . Up to second order, the perturbative expansion for the initial state  $|N_i\rangle$  is

$$|N_i^{(0)}\rangle = |N_i^{(0)}\rangle; \quad (3a)$$

$$|N_i^{(1)}\rangle = \sum_{ab} |ab\rangle \frac{\langle ab|V|N_i^{(0)}\rangle}{\Omega_{N_i} - (E_a + E_b)} + \sum_{abN} |abN^{(0)}N_i^{(0)}\rangle \frac{\langle abN^{(0)}N_i^{(0)}|V|N_i^{(0)}\rangle}{\Omega_{N_i} - (\Omega_{N_i} + \Omega_N + E_a + E_b)}; \quad (3b)$$

$$|N_i^{(2)}\rangle = \sum_{ab} \sum_{a'b'N} |a'b'N^{(0)}\rangle \frac{\langle a'b'N^{(0)}|V|ab\rangle}{\Omega_{N_i} - (E_{a'} + E_{b'} + \Omega_N)} \frac{\langle ab|V|N_i^{(0)}\rangle}{\Omega_{N_i} - (E_a + E_b)} + \sum_{abN} \sum_{a'b'} |a'b'N^{(0)}\rangle \frac{\langle a'b'|V|abN_i^{(0)}\rangle}{\Omega_{N_i} - (E_{a'} + E_{b'} + \Omega_N)} \frac{\langle abN^{(0)}N_i^{(0)}|V|N_i^{(0)}\rangle}{\Omega_{N_i} - (\Omega_{N_i} + \Omega_N + E_a + E_b)}. \quad (3c)$$

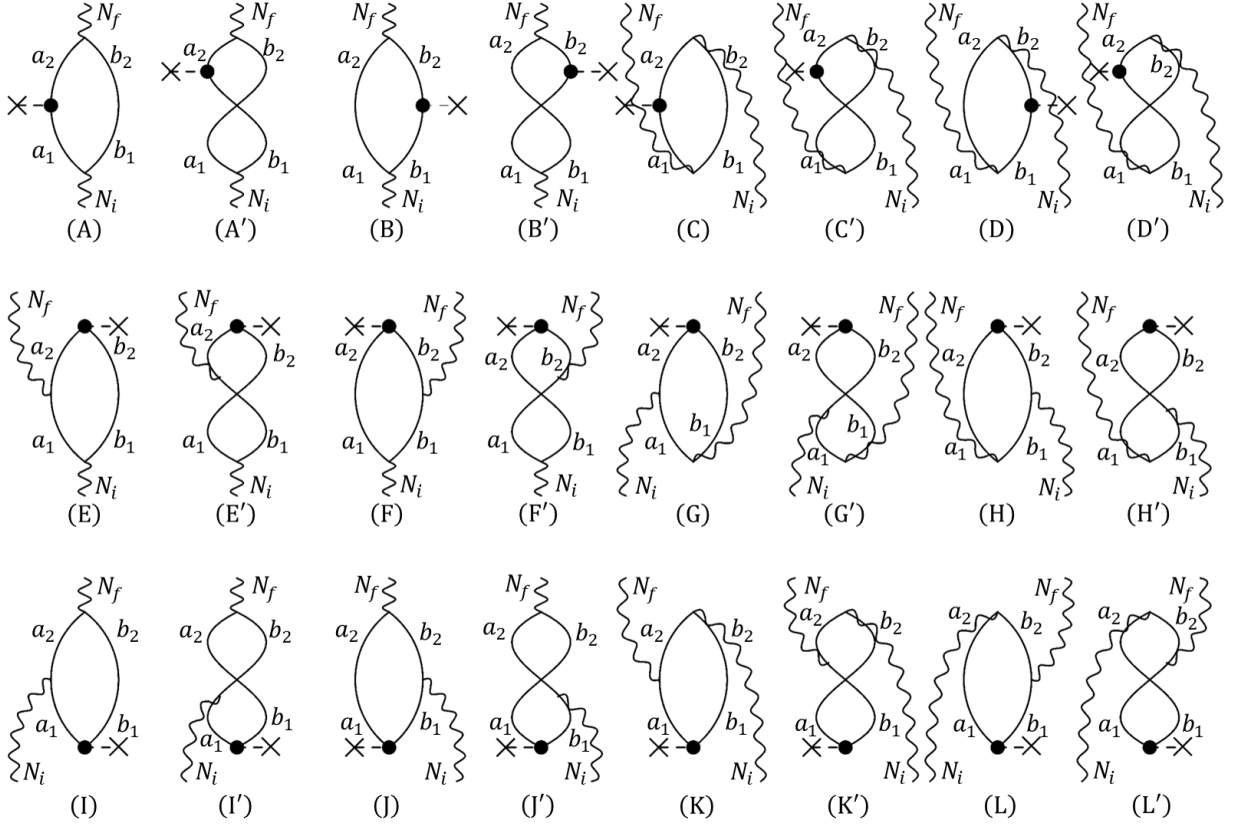


FIG. 2. The 24 second-order NFT diagrams for the  $\gamma$ -decay process between two vibrational states. The cross denotes the external operator  $Q_{\lambda\mu}$ . The shaded circle includes the contribution to  $Q_{\lambda\mu}$  from nuclear polarization.

The diagrams in Fig. 1 provide a graphical representation of the above expressions. For the final state, the expansion is quite similar. We note that terms of pure “bubble” (ring) type in  $|N^{(2)}\rangle$  are not considered, because their resummation is precisely what generates the QRPA phonon  $|N^{(0)}\rangle$ . In addition, some terms in  $|N^{(2)}\rangle$  do not contribute at the second order of the transition matrix element  $\langle N_f | Q_{\lambda\mu} | N_i \rangle$ , owing to a mismatch in the total number of creation and annihilation operators when combining these terms with the one-body transition operator.

The electric multipole operator reads

$$Q_{\lambda\mu} = \sum_{i=1}^A e_i^{\text{eff}} r_i^\lambda Y_{\lambda\mu}(\hat{r}_i), \quad (4)$$

where the effective charge caused by the recoil of the nucleus has been introduced [43]. In the dipole case with  $\lambda = 1$ ,  $e_n^{\text{eff}} = -Z/A$  for the neutron and  $e_p^{\text{eff}} = N/A$  for the proton.

### A. $\gamma$ -decay width in NFT

With the building blocks of the wave functions  $|N\rangle$  [Eq. (3)] and the one-body transition operator  $Q_{\lambda\mu}$  [Eq. (4)], the transition matrix element between vibrational states can be written as

$$\langle N_f | Q_{\lambda\mu} | N_i \rangle = \sum_{k=0}^2 \sum_{k'=0}^2 \langle N_f^{(k')} | Q_{\lambda\mu} | N_i^{(k)} \rangle. \quad (5)$$

In our model, we keep terms up to second order in the interaction  $V$ . The non-vanishing matrix elements of a one-body operator  $Q_{\lambda\mu}$  are of three types: (i) single-quasiparticle transitions:  $\langle a | Q_{\lambda\mu} | b \rangle$ , (ii) quasiparticle-pair creation or annihilation,  $\langle ab | Q_{\lambda\mu} | 0 \rangle$  or  $\langle 0 | Q_{\lambda\mu} | ab \rangle$ , (iii) phonon creation or annihilation,  $\langle N^{(0)} | Q_{\lambda\mu} | 0 \rangle$  or  $\langle 0 | Q_{\lambda\mu} | N^{(0)} \rangle$ . Therefore, we can construct the Feynman

diagrams contributing to the  $\gamma$  decay between two vibrational states in Fig. 2. Note that the phonon creation or annihilation of  $Q_{\lambda\mu}$  will appear in the polarization effect, see Sec. II B.

The reduced transition matrix element at the QRPA level is  $\langle N_f^{(1)} | Q_{\lambda\mu} | N_i^{(1)} \rangle$ , including contributions from diagrams A to D',

$$\langle N_f^{(1)} J_f | Q_{\lambda} | N_i^{(1)} J_i \rangle_{(m)} = \sum_{a_1 b_1 a_2 b_2} X_{a_2 b_2}^{N_f J_f^*} X_{a_1 b_1}^{N_i J_i} \langle (a_2 b_2)_{J_f} | Q_{\lambda} | (a_1 b_1)_{J_i} \rangle_{(m)}, \quad m = A, A', B, B' \quad (6a)$$

$$\langle N_f^{(1)} J_f | Q_{\lambda} | N_i^{(1)} J_i \rangle_{(n)} = (-)^{J_i + J_f + \lambda} \sum_{a_1 b_1 a_2 b_2} Y_{a_2 b_2}^{N_i J_i} Y_{a_1 b_1}^{N_f J_f^*} \langle (a_2 b_2)_{J_i} | Q_{\lambda} | (a_1 b_1)_{J_f} \rangle_{(n)}, \quad n = C, C', D, D' \quad (6b)$$

where  $X_{ab}^{NJ}$  and  $Y_{ab}^{NJ}$  are the forward and backward amplitudes in the QRPA model. The detailed expressions of transition matrix elements  $\langle (a_2 b_2)_{J_2} | Q_{\lambda} | (a_1 b_1)_{J_1} \rangle$  can be found in Appendix A.

The reduced transition matrix elements at QPVC level are  $\langle N_f^{(0)} | Q_{\lambda\mu} | N_i^{(2)} \rangle$  (diagrams E to H') and  $\langle N_f^{(2)} | Q_{\lambda\mu} | N_i^{(0)} \rangle$  (diagrams I to L'),

$$\langle N_f^{(0)} J_f | Q_{\lambda} | N_i^{(2)} J_i \rangle_{(p)} = \hat{f}_i \hat{\lambda}^{-1} \sum_{a_1 b_1} \sum_{a_2 b_2} X_{a_1 b_1}^{N_i J_i} \frac{A_{a_2 b_2(\lambda) N_f, a_1 b_1}^{(3) J_i}(p)}{[\Omega_{N_i} - (\Omega_{N_f} + E_{a_2} + E_{b_2})] + i\eta_1} \langle 0 | Q_{\lambda} | (a_2 b_2)_{\lambda} \rangle, \quad p = E, E', F, F' \quad (7a)$$

$$\langle N_f^{(0)} J_f | Q_{\lambda} | N_i^{(2)} J_i \rangle_{(q)} = \sum_{a_1 b_1} \sum_{a_2 b_2} Y_{a_1 b_1}^{N_f J_f^*} \frac{A_{a_2 b_2, a_1 b_1(J_f) N_i}^{(2) \lambda}(q)}{[\Omega_{N_i} - (\Omega_{N_f} + E_{a_2} + E_{b_2})] + i\eta_1} \langle 0 | Q_{\lambda} | (a_2 b_2)_{\lambda} \rangle, \quad q = G, G', H, H' \quad (7b)$$

$$\langle N_f^{(2)} J_f | Q_{\lambda} | N_i^{(0)} J_i \rangle_{(r)} = (-)^{J_i + J_f + \lambda} \hat{f}_f \hat{\lambda}^{-1} \sum_{a_1 b_1} \sum_{a_2 b_2} X_{a_2 b_2}^{N_f J_f^*} \frac{A_{a_2 b_2, a_1 b_1(\lambda) N_i}^{(2) J_f}(r)}{[\Omega_{N_f} - (\Omega_{N_i} + E_{a_1} + E_{b_1})] - i\eta_1} \langle (a_1 b_1)_{\lambda} | Q_{\lambda} | 0 \rangle, \quad r = I, I', J, J' \quad (7c)$$

$$\langle N_f^{(2)} J_f | Q_{\lambda} | N_i^{(0)} J_i \rangle_{(s)} = (-)^{J_i + J_f + \lambda} \sum_{a_1 b_1} \sum_{a_2 b_2} Y_{a_2 b_2}^{N_i J_i} \frac{A_{a_2 b_2(J_i) N_f, a_1 b_1}^{(3) \lambda}(s)}{[\Omega_{N_f} - (\Omega_{N_i} + E_{a_1} + E_{b_1})] - i\eta_1} \langle (a_1 b_1)_{\lambda} | Q_{\lambda} | 0 \rangle, \quad s = K, K', L, L' \quad (7d)$$

where  $\hat{J} = \sqrt{2J+1}$ . The imaginary part  $\eta_1$  in the energy denominator takes into account the coupling to more complicated configurations not included in our model space. The detailed expressions for the quasiparticle transition matrix elements, as well as the QPVC matrix elements  $A^{(2)}$  and  $A^{(3)}$  can be found in Appendix A and B. Diagrams E to H' correspond to the process of initial phonon  $|N_i\rangle$  scattering into  $|a_2 b_2 N_f\rangle$ . Therefore, they will contribute significantly if the initial GDR state includes configurations with 2qp coupled with the final  $2_1^+$  state in its wave function. The polarization effect will be presented in Sec. II B.

By considering the 24 diagrams sketched in Fig. 2, the transition strength can be calculated as

$$B_{\gamma}^{fi} = \frac{1}{2J_i + 1} \left| \sum_{n=A, \dots, L'} \langle N_f | Q_{\lambda} | N_i \rangle_{(n)} \right|^2. \quad (8)$$

The corresponding  $\gamma$ -decay width  $\Gamma_{\gamma}$  is

$$\Gamma_{\gamma} = \frac{1}{4\pi\epsilon_0} \frac{8\pi(\lambda+1)}{\lambda [(2\lambda+1)!!]^2} \left( \frac{\Delta E}{\hbar c} \right)^{2\lambda+1} B_{\gamma}^{fi}, \quad (9)$$

where  $\Delta E = \Omega_{N_i} - \Omega_{N_f}$  represents the transition energy.

## B. Polarization effect

The large transition moment of  $Q_{\lambda\mu}$  with  $\lambda = 1$  will induce nuclear vibrations [44]. As a result, the initial and final states,  $N_i$  and  $N_f$  are clothed in a cloud of quanta. This, in turn, gives rise to important modifications to the transition moment. We deal with this kind of polarization effect using a factorization approach, as sketched in Fig. 3. The matrix element of  $Q_{\lambda\mu}$  between the clothed phonons is

$$\langle N_f | Q_{\lambda\mu}^{\text{pol}} | N_i \rangle \equiv \langle \tilde{N}_f | Q_{\lambda\mu} | \tilde{N}_i \rangle = \langle N_f | Q_{\lambda\mu} | N_i \rangle + \sum_{\nu} \frac{\langle 0 | Q_{\lambda\mu} | \nu \rangle \langle N_f \nu | V | N_i \rangle}{\Omega_{N_i} - (\Omega_{N_f} + \Omega_{\nu})} + \frac{\langle N_f | V | N_i \nu \rangle \langle \nu | Q_{\lambda\mu} | 0 \rangle}{\Omega_{N_f} - (\Omega_{N_i} + \Omega_{\nu})}. \quad (10)$$

Second, we further consider the interaction between phonon and individual quasiparticles, so that we insert the expansion of  $N_i$  and  $N_f$  in Eq. (3) into Eq. (10). We take diagrams A, E, and I as examples, because they are the diagrams that typically come from  $\langle N_f^{(1)} || \mathcal{Q}_{\lambda\mu} || N_i^{(1)} \rangle$ ,  $\langle N_f^{(0)} || \mathcal{Q}_{\lambda\mu} || N_i^{(2)} \rangle$ , and  $\langle N_f^{(2)} || \mathcal{Q}_{\lambda\mu} || N_i^{(0)} \rangle$ , respectively. After considering the polarization effect they become

$$\begin{aligned} \langle N_f^{(1)} || \mathcal{Q}_{\lambda}^{\text{pol}} || N_i^{(1)} \rangle_{(A)} &= \langle N_f^{(1)} || \mathcal{Q}_{\lambda} || N_i^{(1)} \rangle_{(A)} + \hat{\lambda}^{-1} \sum_{\nu} (-)^{J_i+J_f+\lambda} \hat{f}_i \frac{\langle 0 || \mathcal{Q}_{\lambda} || \nu \rangle X_{a_2 b_2}^{N_f J_f^*} [A_{a_2 b_2 (J_f) \nu, a_1 b_1}^{(3) J_i} (1)] X_{a_1 b_1}^{N_i J_i}}{[\Omega_{N_i} - (\Omega_{N_f} + \Omega_{\nu}) + i\eta_2]} \\ &+ \hat{f}_f \frac{X_{a_2 b_2}^{N_f J_f^*} [A_{a_2 b_2, a_1 b_1 (J_i) \nu}^{(2) J_f} (1)] X_{a_1 b_1}^{N_i J_i} \langle \nu || \mathcal{Q}_{\lambda} || 0 \rangle}{[\Omega_{N_f} - (\Omega_{N_i} + \Omega_{\nu}) - i\eta_2]}, \end{aligned} \quad (11)$$

$$\begin{aligned} \langle N_f^{(0)} || \mathcal{Q}_{\lambda}^{\text{pol}} || N_i^{(2)} \rangle_{(E)} &= \langle N_f^{(0)} || \mathcal{Q}_{\lambda} || N_i^{(2)} \rangle_{(E)} + \hat{\lambda}^{-1} \sum_{\nu} \frac{\langle 0 || \mathcal{Q}_{\lambda} || \nu \rangle \langle \nu || V || a_2 b_2 \rangle [A_{a_2 b_2 (\lambda) N_f, a_1 b_1}^{(3) J_i} (1)] X_{a_1 b_1}^{N_i J_i}}{[\Omega_{N_i} - (\Omega_{N_f} + \Omega_{\nu}) + i\eta_2] [\Omega_{N_i} - (E_{a_2} + E_{b_2} + \Omega_{N_f})]} \\ &+ \frac{\langle 0 || V || a_2 b_2 \nu \rangle [A_{a_2 b_2 (\lambda) N_f, a_1 b_1}^{(3) J_i} (1)] X_{a_1 b_1}^{N_i J_i} \langle \nu || \mathcal{Q}_{\lambda} || 0 \rangle}{[\Omega_{N_f} - (\Omega_{N_i} + \Omega_{\nu}) - i\eta_2] [\Omega_{N_i} - (E_{a_2} + E_{b_2} + \Omega_{N_f})]}, \end{aligned} \quad (12)$$

$$\begin{aligned} \langle N_f^{(2)} || \mathcal{Q}_{\lambda}^{\text{pol}} || N_i^{(0)} \rangle_{(I)} &= \langle N_f^{(2)} || \mathcal{Q}_{\lambda} || N_i^{(0)} \rangle_{(I)} + \hat{\lambda}^{-1} \sum_{\nu} \frac{\langle 0 || \mathcal{Q}_{\lambda} || \nu \rangle X_{a_2 b_2}^{N_f J_f^*} [A_{a_2 b_2, a_1 b_1 (\lambda) N_i}^{(2) J_f} (1)] \langle a_1 b_1 \nu || V || 0 \rangle}{[\Omega_{N_i} - (\Omega_{N_f} + \Omega_{\nu}) + i\eta_2] [\Omega_{N_f} - (E_{a_1} + E_{b_1} + \Omega_{N_i})]} \\ &+ \frac{X_{a_2 b_2}^{N_f J_f^*} [A_{a_2 b_2, a_1 b_1 (\lambda) N_i}^{(2) J_f} (1)] \langle a_1 b_1 || V || \nu \rangle \langle \nu || \mathcal{Q}_{\lambda} || 0 \rangle}{[\Omega_{N_f} - (\Omega_{N_i} + \Omega_{\nu}) - i\eta_2] [\Omega_{N_f} - (E_{a_1} + E_{b_1} + \Omega_{N_i})]}. \end{aligned} \quad (13)$$

Figure 4 represents the above expressions in a diagrammatic way. The imaginary part  $\eta_2$  accounts for damping of the phonon  $\nu$ . Expressions of the QRPA vertices  $\langle \nu || V || ab \rangle$  and  $\langle ab, \nu || V || 0 \rangle$  are presented in Appendix C. Polarization corrections in the remaining diagrams can be obtained analogously.

By comparing the above equations with Eqs. (6) and (7), the polarization effect can be included in the transition matrix elements of quasiparticles. For diagrams A to D', the polarized transition matrix elements are

$$\begin{aligned} \langle (a_2 b_2)_{J_2} || \mathcal{Q}_{\lambda}^{\text{pol}} || (a_1 b_1)_{J_1} \rangle_{(m)} &= \langle (a_2 b_2)_{J_2} || \mathcal{Q}_{\lambda} || (a_1 b_1)_{J_1} \rangle_{(m)} \\ &+ \hat{\lambda}^{-1} \sum_{\nu} (-)^{J_1+J_2+\lambda} \hat{f}_1 \frac{\langle 0 || \mathcal{Q}_{\lambda} || \nu \rangle [A_{a_2 b_2 (J_2) \nu, a_1 b_1}^{(3) J_1} (n)]}{\Omega_{N_i} - (\Omega_{N_f} + \Omega_{\nu}) + i\eta_2} + \hat{f}_2 \frac{[A_{a_2 b_2, a_1 b_1 (J_1) \nu}^{(2) J_2} (n)] \langle \nu || \mathcal{Q}_{\lambda} || 0 \rangle}{\Omega_{N_f} - (\Omega_{N_i} + \Omega_{\nu}) - i\eta_2}, \end{aligned} \quad (14a)$$

where  $m = A, A', B, B'$  and  $m = C, C', D, D'$  correspond to  $n = 1, 2, 3, 4$ .

For diagrams E to H', and I to L', the polarized transition matrix elements are respectively

$$\langle 0 || \mathcal{Q}_{\lambda}^{\text{pol}} || (a_2 b_2)_{\lambda} \rangle = \langle 0 || \mathcal{Q}_{\lambda} || (a_2 b_2)_{\lambda} \rangle + \hat{\lambda}^{-1} \sum_{\nu} \frac{\langle 0 || \mathcal{Q}_{\lambda} || \nu \rangle \langle \nu || V || a_2 b_2 \rangle}{\Omega_{N_i} - (\Omega_{N_f} + \Omega_{\nu}) + i\eta_2} + \frac{\langle 0 || V || a_2 b_2 \nu \rangle \langle \nu || \mathcal{Q}_{\lambda} || 0 \rangle}{\Omega_{N_f} - (\Omega_{N_i} + \Omega_{\nu}) - i\eta_2}, \quad (15a)$$

$$\langle (a_1 b_1)_{\lambda} || \mathcal{Q}_{\lambda}^{\text{pol}} || 0 \rangle = \langle (a_1 b_1)_{\lambda} || \mathcal{Q}_{\lambda} || 0 \rangle + \hat{\lambda}^{-1} \sum_{\nu} \frac{\langle 0 || \mathcal{Q}_{\lambda} || \nu \rangle \langle a_1 b_1 \nu || V || 0 \rangle}{\Omega_{N_i} - (\Omega_{N_f} + \Omega_{\nu}) + i\eta_2} + \frac{\langle a_1 b_1 || V || \nu \rangle \langle \nu || \mathcal{Q}_{\lambda} || 0 \rangle}{\Omega_{N_f} - (\Omega_{N_i} + \Omega_{\nu}) - i\eta_2}. \quad (15b)$$

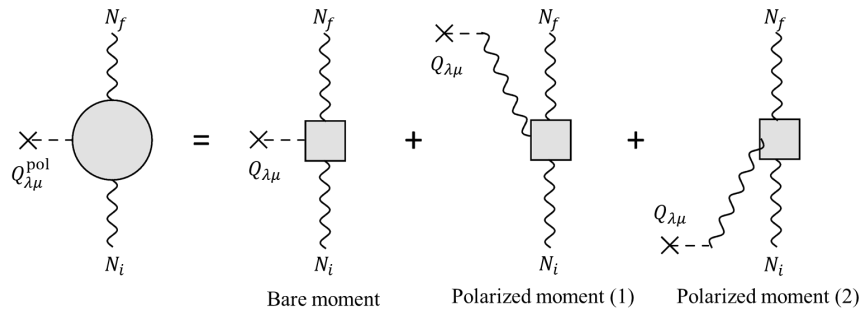


FIG. 3. Diagrammatic representation of the polarization effect. The shaded square denotes the perturbative process shown in Fig. 2.

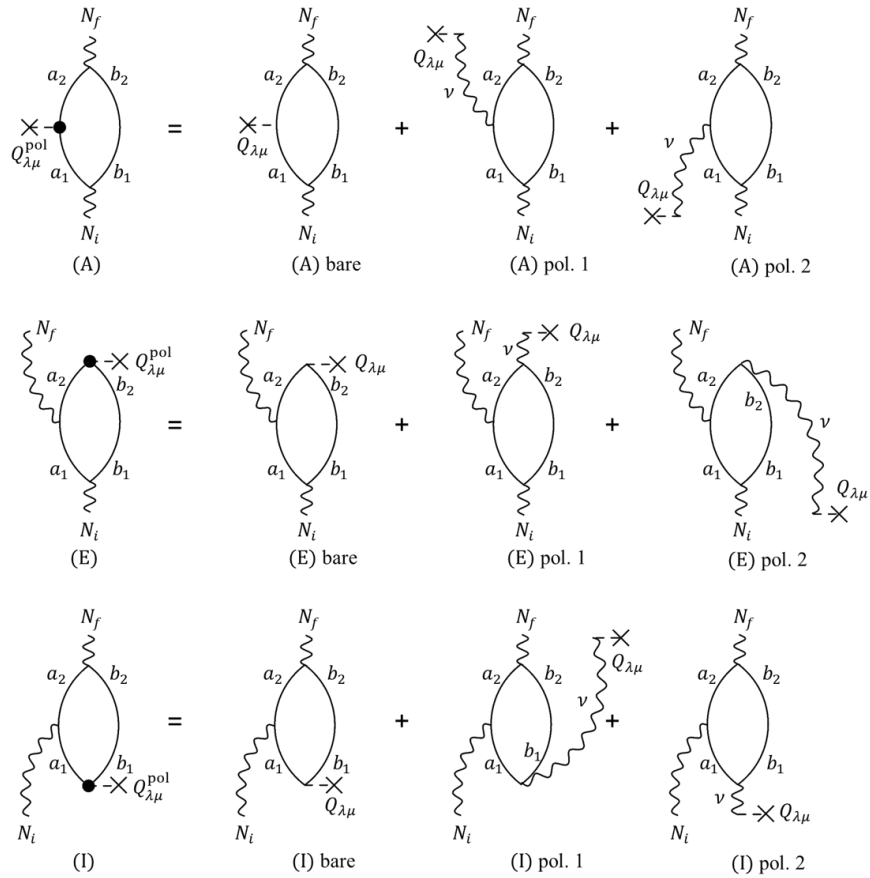


FIG. 4. The polarization effect in diagram A, E, and I.

### III. NUMERICAL DETAILS

The phonon states are calculated with the self-consistent QRPA model. The box size for calculating the single-particle levels is 20 fm. A smooth cut-off of 60 MeV is applied to the equivalent Hartree-Fock energy of the quasiparticle states, having a Fermi profile of diffuseness 0.1 MeV. Volume pairing is adopted consistently in HFB, in the QRPA calculation, and in all the vertices of the diagrams. Its strength is adjusted to reproduce the experimental pairing gaps obtained from the three-point formula of binding energies. The values for the volume pairing strengths are respectively  $-206.1 \text{ MeV}\cdot\text{fm}^3$ ,  $-198.1 \text{ MeV}\cdot\text{fm}^3$ ,  $-186.7 \text{ MeV}\cdot\text{fm}^3$ , and  $-182.9 \text{ MeV}\cdot\text{fm}^3$  for SIII, SGII, SkM\*, and LNS. The model space is sufficiently large to exhaust 100.1% of the isovector energy-weighted sum rule when using the SIII interaction. The GDR states are chosen from the QRPA states within the energy range of 10-18 MeV, requiring a fraction of isovector (IV) non-energy-weighted sum rule (NEWSR) larger than 5%. The selection criteria for the dipole modes that contribute to the polarization effect are IV or isoscalar (IS) NEWSR fraction larger than 5% and energy smaller than 30 MeV. We note that the polarization effect from IS phonons can be neglected as one may expect.

We investigate the stability of the results against variation of the two imaginary parts  $\eta_1$  and  $\eta_2$  by studying the sensitivity of  $\sum \Gamma_\gamma$  to their values. Here  $\sum \Gamma_\gamma$  is the summed  $\gamma$ -decay width to the  $2_1^+$  state for the selected dipole modes within the GDR region. As shown in Fig. 5, the  $\gamma$ -decay width is relatively stable for  $\eta_1$  and  $\eta_2$  around 2.2 MeV. The similar dependence of  $\sum \Gamma_\gamma$  on  $\eta_1$  and on  $\eta_2$  is not accidental, because both of them enter the denominators in a similar way and mimic the phonon damping. Therefore, it is reassuring that we have stability with respect to  $\eta_1$  and  $\eta_2$  in a region that corresponds to the physical value, namely half of the experimental GDR width in  $^{140}\text{Ce}$  [45].

### IV. RESULTS AND DISCUSSIONS

The transition amplitude  $\langle N_f J_f || Q_\lambda || N_i J_i \rangle$  involves both the initial and final states. Therefore, we first assess the quality of the theoretical description of the  $2_1^+$  state and GDR. The experimental excitation energies and  $B(E2)$  value, along with the QRPA

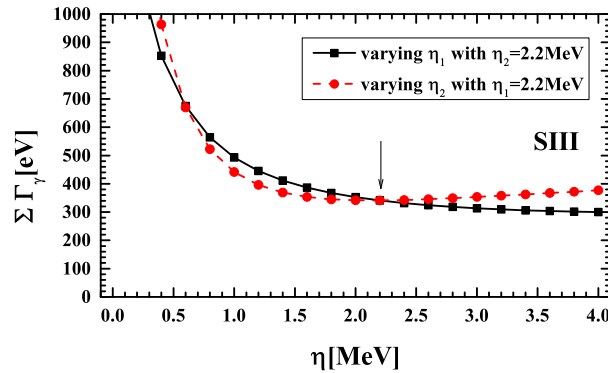


FIG. 5. Stability of the results for the  $\gamma$ -decay width against variation of the imaginary parts  $\eta_1$  and  $\eta_2$ .  $\Sigma\Gamma_\gamma$  denotes the sum of the  $\gamma$ -decay width to the  $2_1^+$  state for the selected dipole modes in GDR region. Black (red) line shows the result of varying  $\eta_1$  ( $\eta_2 = 2.2$  MeV) while keeping  $\eta_1 = 2.2$  MeV ( $\eta_2 = 2.2$  MeV).

TABLE I. Experimental [46] and theoretical excitation energies and  $E2$  transition strengths of the  $2_1^+$  state in  $^{140}\text{Ce}$ . The energies of the GDR are listed in the last line, where the experimental value is obtained via standard Lorentzian fitting to the photoneutron cross section [45], while the theoretical ones are obtained by  $m_1(E1)/m_0(E1)$ .

	Expt.	SIII	SGII	SkM*	LNS
$E(2_1^+)$ [MeV]	1.60	2.50	2.10	1.80	2.03
$B(E2)_{2_1^+}$ [ $10^4 e^2 \text{fm}^2$ ]	0.304	0.300	0.389	0.463	0.349
$E(\text{GDR})$ [MeV]	15.03	16.30	15.20	15.47	15.66

results calculated with SIII [47], SGII [48], SkM\* [49], and LNS [50] Skyrme functionals, are listed in Table I. The theoretical GDR energy is calculated by the ratio of energy-weighted sum rule to the non-energy-weighted sum rule  $m_1(E1)/m_0(E1)$ , where the states in 8 to 28 MeV are included to match the Lorentzian fitting range of the experimental photoneutron cross section. The  $E1$  strength distributions of the 4 Skyrme functionals are depicted in Fig. 6. For the SIII functional, the energies for both  $2_1^+$  and GDR are slightly higher than the experimental ones, while the  $B(E2)$  value for  $2_1^+$  is reproduced very well. SGII, SkM\*, and LNS functionals provide a better description of the excitation energies than SIII, although they overestimate the  $B(E2)$  value of the  $2_1^+$  state. Overall, these 4 Skyrme functionals provide a reasonable description of both the  $2_1^+$  state and the GDR, and can thus be employed in the subsequent calculations of  $\gamma$ -decay.

Table II presents the  $\gamma$ -decay properties from the selected GDR states to the first  $2_1^+$  state in  $^{140}\text{Ce}$  calculated by SIII, SGII, SkM\*, and LNS functionals. For each functional, the excitation energy  $E$  of the single GDR state, the corresponding partial  $\gamma$ -decay width to the  $2_1^+$  state,  $\Gamma_\gamma^{2_1^+}$ , and the branching ratio are listed. The total decay width  $\Sigma\Gamma_\gamma^{2_1^+}$  varies from 216 eV (LNS)

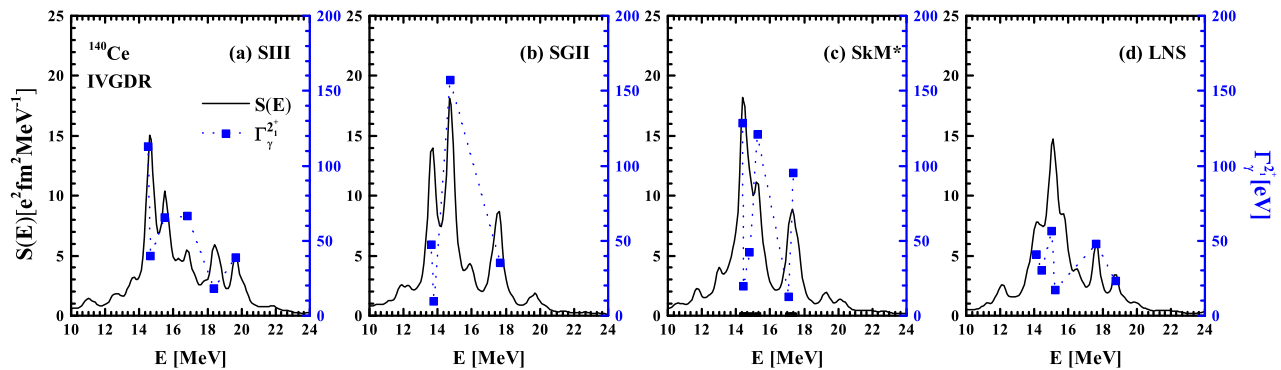


FIG. 6.  $E1$  transition strength distributions (black lines) around the GDR region calculated by the QRPA model with SIII (a), SGII (b), SkM\* (c), and LNS (d) interactions. The width parameter  $\Gamma$  of the Lorentzian function is set as 0.5 MeV to resolve the individual peaks clearly. The partial  $\gamma$ -decay width to  $2_1^+$  state  $\Gamma_\gamma^{2_1^+}$  (blue square) of individual GDR states is also shown in the figure.

TABLE II.  $\gamma$ -decay widths and the branching ratios of the selected GDR states. The ratio  $R$  for individual GDR state is calculated by  $\Gamma_{\gamma}^{2+}/\Gamma_{\gamma}^{\text{g.s.}}$ . The total ratio  $R$  is calculated by  $\sum \Gamma_{\gamma}^{2+}/\sum \Gamma_{\gamma}^{\text{g.s.}}$ .

SIII				SGII				SkM*				LNS			
$E$ [MeV]	$\Gamma_{\gamma}^{2+}$ [eV]	$\Gamma_{\gamma}^{\text{g.s.}}$ [eV]	$R$ [%]	$E$ [MeV]	$\Gamma_{\gamma}^{2+}$ [eV]	$\Gamma_{\gamma}^{\text{g.s.}}$ [eV]	$R$ [%]	$E$ [MeV]	$\Gamma_{\gamma}^{2+}$ [eV]	$\Gamma_{\gamma}^{\text{g.s.}}$ [eV]	$R$ [%]	$E$ [MeV]	$\Gamma_{\gamma}^{2+}$ [eV]	$\Gamma_{\gamma}^{\text{g.s.}}$ [eV]	$R$ [%]
14.53	112.9	2952.9	3.82	13.62	47.5	4029.6	1.18	14.38	128.3	8209.0	1.56	14.13	40.9	2790.4	1.47
14.65	39.8	9174.5	0.43	13.77	9.5	2624.9	0.36	14.45	19.6	3642.8	0.54	14.42	30.1	2282.5	1.32
15.50	65.4	7491.7	0.87	14.73	157.3	12744.4	1.23	14.78	42.4	4084.2	1.04	15.02	56.3	6966.4	0.81
16.84	66.4	4400.8	1.51	17.65	35.5	6937.5	0.51	15.26	120.8	7547.8	1.60	15.22	17.1	2682.0	0.64
18.37	18.0	6532.9	0.28					17.10	12.7	5141.9	0.25	17.63	48.0	8215.3	0.58
19.65	38.6	8592.5	0.45					17.34	95.2	6887.4	1.38	18.76	23.4	5183.9	0.45
Total	341.0	39145.2	0.87	Total	249.9	26336.5	0.95	Total	419.0	35513.1	1.18	Total	215.8	28120.5	0.77

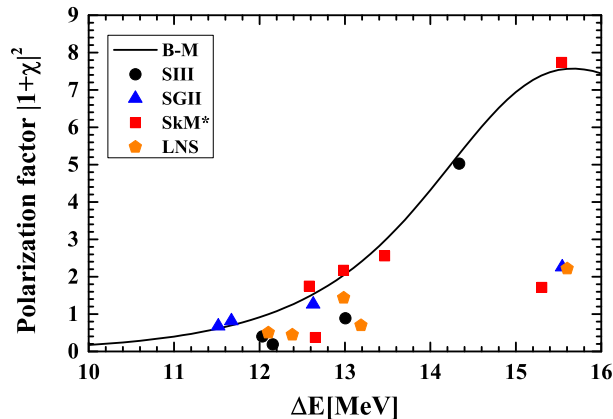


FIG. 7. Polarization factor as a function of the transition energy  $\Delta E = \Delta\Omega_{if}$ . The solid line is Bohr-Mottelson formula with experimental GDR energy and width. The points are calculated by our model for the dipole states lying in the GDR region with different Skyrme functionals.

to 419 eV (SkM\*), while the total branching ratio ranges from 0.77% to 1.18%. The state-by-state values of  $\Gamma_{\gamma}^{2+}$  are shown as blue squares in Fig. 6. Overall,  $\Gamma_{\gamma}^{2+}$  shows a similar energy dependence to the  $E1$  strength, exhibiting enhanced values around the main IVGDR peak.

In Fig. 7, we present the polarization factor,  $|1 + \chi|^2$ , as a function of the transition energy  $\Delta E = \Delta\Omega_{if}$ , in the GDR region in  $^{140}\text{Ce}$ . In our model, the polarization factor  $|1 + \chi|^2$  is calculated as the ratio of the  $\gamma$ -decay width with and without the polarization correction. Macroscopically, the dipole polarizability  $\chi$  can be calculated by the Bohr-Mottelson (B-M) formula [18, 44]

$$\chi = \frac{-0.76E_{\text{GDR}}^2}{(E_{\text{GDR}} + \Delta E + i\Gamma_{\text{D}}/2)(E_{\text{GDR}} - \Delta E - i\Gamma_{\text{GDR}}/2)}, \quad (16)$$

where the experimental values  $E_{\text{GDR}} = 15.03$  MeV and  $\Gamma_{\text{GDR}} = 4.4$  MeV are used. The polarization factors calculated from the microscopic model generally follow the trend predicted by the macroscopic B-M formula. As the transition energy  $\Delta E$  is well below the GDR energy, the factor is smaller than 1, indicating that the polarization suppresses the  $\gamma$ -decay width. When  $\Delta E$  increases and approaches the resonance region, the factor exceeds 1, implying that the polarization now enhances the decay width. A maximum enhancement can be reached when  $\Delta E$  is comparable to the GDR energy, where the virtual excitation of the collective mode is most efficient [44]. We note that there are some deviations from the B-M curve for several individual dipole states, arising from the more detailed treatment in our microscopic approach. Namely, the B-M formula essentially models the polarization effect mediated by a single collective GDR phonon, while our calculation includes the contributions from several fragmented dipole phonon states.

## V. SUMMARY

In summary, we have developed a fully self-consistent Skyrme QPVC model to calculate the  $\gamma$  decay between vibrational states in superfluid nuclei. We treat the initial and final states as QRPA phonons. Then, within the framework of nuclear field theory,



we consider the perturbation expansion of the phonon wave functions, induced by the interaction between quasiparticles and phonons, to ensure a comprehensive treatment of the many-body dynamics. Moreover, we consider the important polarization effect. The self-consistency of our model lies in employing the same Skyrme force and pairing interaction, without further adjustable parameters, both in the ground state, in the construction of the phonons, and in the interaction vertices.

Motivated by recent experiments at the HIγS [40], we apply our model to the  $\gamma$ -decay from the GDR to the  $2_1^+$  state in  $^{140}\text{Ce}$ , with SIII, SGII, SkM\* and LNS functionals. The properties of both the GDR and the  $2_1^+$  state are reasonably reproduced. For the decay process, we calculate the partial and total  $\gamma$ -decay widths of individual dipole modes within the GDR region. The total width ranges from approximately 200 to 420 eV, and the corresponding branching ratio varies between 0.75% and 1.20%, depending on the functional. Furthermore, the polarization factor extracted from our microscopic model is compared with the Bohr-Mottelson formula. Both approaches yield the same increasing trend with the transition energy.

## ACKNOWLEDGEMENTS

W.-L. L. acknowledges helpful discussions with Zheng-Zheng Li and Yi-Wei Hao. Y.-F. N. and G. C. acknowledge helpful discussions with Norbert Pietralla, Johann Isaak and the group at TU Darmstadt. This work was supported by the ‘‘Young Scientist Scheme’’ of National Key Research and Development (R&D) Program under grant No. 2021YFA1601500, the National Natural Science Foundation of China under grant Nos. 12405135, 12447168, 12075104, 12447106, the Science and Technology Innovation Leading Talent Project of Gansu Province (25RCCKA025), the Lingchuang Research Project of China National Nuclear Corporation (CNNC-LCKY-2024-082), the Fundamental Research Funds for the Central Universities (lzujbky-2023-stlt01).

## Appendix A: Quasiparticle transition matrix elements

In the quasiparticle picture, the one-body operator can be written as

$$Q_{\lambda\mu} = \sum_{ab} \sum_{m_a m_b} \hat{\lambda}^{-1} C_{j_a m_a j_b m_b}^{\lambda\mu} \langle j_a || Q_{\lambda} || j_b \rangle (-u_a v_b \alpha_a^{\dagger} \alpha_b^{\dagger} + u_a u_b \alpha_a^{\dagger} \alpha_b^{\dagger} - v_a v_b \alpha_{\bar{a}} \alpha_{\bar{b}}^{\dagger} + v_a u_b \alpha_{\bar{a}} \alpha_{\bar{b}}), \quad (\text{A1})$$

where we use the special Bogoliubov transformation from particle to quasiparticle.

The two terms  $\alpha_a^{\dagger} \alpha_b^{\dagger}$  and  $\alpha_{\bar{a}} \alpha_{\bar{b}}^{\dagger}$  in  $Q_{\lambda\mu}$  result in 8 different contractions in the transition matrix element  $\langle (a_2 b_2)_{J_2} || Q_{\lambda} || (a_1 b_1)_{J_1} \rangle$  [51],

$$\langle (a_2 b_2)_{J_2} || Q_{\lambda} || (a_1 b_1)_{J_1} \rangle_{(1)} = \mathcal{N}_{a_1 b_1}^{J_1} \mathcal{N}_{a_2 b_2}^{J_2} \hat{J}_1 \hat{J}_2 \delta_{b_1 b_2} u_{a_2} u_{a_1} (-)^{j_{a_2} + j_{b_1} + J_1 + \lambda} \langle j_{a_2} || Q_{\lambda} || j_{a_1} \rangle \left\{ \begin{matrix} j_{a_2} & j_{a_1} & \lambda \\ J_1 & J_2 & j_{b_1} \end{matrix} \right\}, \quad (\text{A2})$$

$$\langle (a_2 b_2)_{J_2} || Q_{\lambda} || (a_1 b_1)_{J_1} \rangle_{(2)} = \mathcal{N}_{a_1 b_1}^{J_1} \mathcal{N}_{a_2 b_2}^{J_2} \hat{J}_1 \hat{J}_2 \delta_{a_1 b_2} u_{a_2} u_{b_1} (-)^{j_{a_2} + j_{b_1} + \lambda} \langle j_{a_2} || Q_{\lambda} || j_{b_1} \rangle \left\{ \begin{matrix} j_{a_2} & j_{b_1} & \lambda \\ J_1 & J_2 & j_{a_1} \end{matrix} \right\}, \quad (\text{A3})$$

$$\langle (a_2 b_2)_{J_2} || Q_{\lambda} || (a_1 b_1)_{J_1} \rangle_{(3)} = \mathcal{N}_{a_1 b_1}^{J_1} \mathcal{N}_{a_2 b_2}^{J_2} \hat{J}_1 \hat{J}_2 \delta_{a_1 a_2} u_{b_2} u_{b_1} (-)^{j_{b_1} + j_{a_2} + J_2 + \lambda} \langle j_{b_2} || Q_{\lambda} || j_{b_1} \rangle \left\{ \begin{matrix} j_{b_2} & j_{b_1} & \lambda \\ J_1 & J_2 & j_{a_1} \end{matrix} \right\}, \quad (\text{A4})$$

$$\langle (a_2 b_2)_{J_2} || Q_{\lambda} || (a_1 b_1)_{J_1} \rangle_{(4)} = \mathcal{N}_{a_1 b_1}^{J_1} \mathcal{N}_{a_2 b_2}^{J_2} \hat{J}_1 \hat{J}_2 \delta_{b_1 a_2} u_{b_2} u_{a_1} (-)^{J_1 + J_2 + \lambda + 1} \langle j_{b_2} || Q_{\lambda} || j_{a_1} \rangle \left\{ \begin{matrix} j_{b_2} & j_{a_1} & \lambda \\ J_1 & J_2 & j_{b_1} \end{matrix} \right\}, \quad (\text{A5})$$

$$\langle (a_2 b_2)_{J_2} || Q_{\lambda} || (a_1 b_1)_{J_1} \rangle_{(5)} = \mathcal{N}_{a_1 b_1}^{J_1} \mathcal{N}_{a_2 b_2}^{J_2} \hat{J}_1 \hat{J}_2 \delta_{b_1 b_2} v_{a_1} v_{a_2} \langle j_{a_1} || Q_{\lambda} || j_{a_2} \rangle (-)^{j_{a_1} + j_{b_1} + J_1 + 1} \left\{ \begin{matrix} j_{a_2} & j_{a_1} & \lambda \\ J_1 & J_2 & j_{b_1} \end{matrix} \right\}, \quad (\text{A6})$$

$$\langle (a_2 b_2)_{J_2} || Q_{\lambda} || (a_1 b_1)_{J_1} \rangle_{(6)} = \mathcal{N}_{a_1 b_1}^{J_1} \mathcal{N}_{a_2 b_2}^{J_2} \hat{J}_1 \hat{J}_2 \delta_{a_1 b_2} v_{a_2} v_{b_1} \langle j_{b_1} || Q_{\lambda} || j_{a_2} \rangle \left\{ \begin{matrix} j_{a_2} & j_{b_1} & \lambda \\ J_1 & J_2 & j_{a_1} \end{matrix} \right\}, \quad (\text{A7})$$

$$\langle (a_2 b_2)_{J_2} || Q_{\lambda} || (a_1 b_1)_{J_1} \rangle_{(7)} = \mathcal{N}_{a_1 b_1}^{J_1} \mathcal{N}_{a_2 b_2}^{J_2} \hat{J}_1 \hat{J}_2 \delta_{a_1 a_2} v_{b_2} v_{b_1} (-)^{j_{a_2} + j_{b_2} + J_2 + 1} \langle j_{b_1} || Q_{\lambda} || j_{b_2} \rangle \left\{ \begin{matrix} j_{b_2} & j_{b_1} & \lambda \\ J_1 & J_2 & j_{a_1} \end{matrix} \right\}, \quad (\text{A8})$$

$$\langle (a_2 b_2)_{J_2} \| Q_\lambda \| (a_1 b_1)_{J_1} \rangle_{(8)} = \mathcal{N}_{a_1 b_1}^{J_1} \mathcal{N}_{a_2 b_2}^{J_2} \hat{J}_1 \hat{J}_2 \delta_{b_1 a_2} v_{b_2} v_{a_1} (-)^{j_{a_1} + j_{b_2} + J_1 + J_2 + 1} \langle j_{a_1} \| Q_\lambda \| j_{b_2} \rangle \left\{ \begin{matrix} j_{b_2} & j_{a_1} & \lambda \\ J_1 & J_2 & j_{b_1} \end{matrix} \right\}, \quad (\text{A9})$$

where  $\mathcal{N}_{ab}^J$  is a normalization factor,

$$\mathcal{N}_{ab}^J = \frac{\sqrt{1 + (-)^J \delta_{ab}}}{1 + \delta_{ab}}. \quad (\text{A10})$$

Diagrams A and C corresponds to  $\langle (a_2 b_2)_{J_2} \| Q_\lambda \| (a_1 b_1)_{J_1} \rangle_{[(1)+(5)]}$ , where there is a  $\delta_{b_1 b_2}$ . Diagrams A' and C' corresponds to  $\langle (a_2 b_2)_{J_2} \| Q_\lambda \| (a_1 b_1)_{J_1} \rangle_{[(2)+(6)]}$ , where there is a  $\delta_{a_1 b_2}$ . Diagrams B and D corresponds to  $\langle (a_2 b_2)_{J_2} \| Q_\lambda \| (a_1 b_1)_{J_1} \rangle_{[(3)+(7)]}$ , where there is a  $\delta_{a_1 a_2}$ . Diagrams B' and D' corresponds to  $\langle (a_2 b_2)_{J_2} \| Q_\lambda \| (a_1 b_1)_{J_1} \rangle_{[(4)+(8)]}$ , where there is a  $\delta_{b_1 a_2}$ .

The other two terms  $\alpha_{\bar{a}}^\dagger \alpha_{\bar{b}}$  and  $\alpha_a^\dagger \alpha_b^\dagger$  in  $Q_{\lambda\mu}$  lead to the quasiparticle-pair annihilation and creation,

$$\langle 0 \| Q_\lambda \| (ab)_\lambda \rangle = \mathcal{N}_{ab}^\lambda [(-)^{j_a + j_b + \lambda} v_b u_a \langle j_b \| Q_\lambda \| j_a \rangle - v_a u_b \langle j_a \| Q_\lambda \| j_b \rangle], \quad (\text{A11})$$

$$\langle (ab)_\lambda \| Q_\lambda \| 0 \rangle = \mathcal{N}_{ab}^\lambda [-\langle j_a \| Q_\lambda \| j_b \rangle u_a v_b + (-)^{j_a + j_b + \lambda} \langle j_b \| Q_\lambda \| j_a \rangle u_b v_a], \quad (\text{A12})$$

which are involved in diagrams E to H' and diagrams I to L' respectively.

### Appendix B: QPVC matrix elements

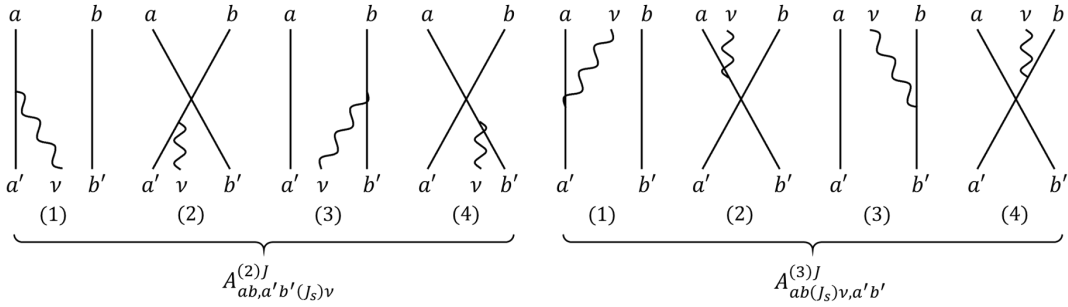


FIG. 8. Diagrams for the QPVC matrix elements  $A_{ab,a'b'(J_s)v}^{(2)J}$  and  $A_{ab(J_s)v,a'b'}^{(3)J}$ .

The QPVC matrix elements  $A^{(2)}$  and  $A^{(3)}$  are

$$A_{ab,a'b'(J_s)v}^{(2)JM} = \langle 0 | [A_{ab}(JM), [V, B_{a'b'(J_s)v}^\dagger(JM)]] | 0 \rangle, \quad (\text{B1})$$

$$A_{ab(J_s)v,a'b'}^{(3)JM} = \langle 0 | [B_{ab(J_s)v}(JM), [V, A_{a'b'}^\dagger(JM)]] | 0 \rangle, \quad (\text{B2})$$

where  $A^\dagger$  creates a quasiparticle-pair state (2qp), and  $B^\dagger$  creates a 2qp $\otimes$ phonon state,

$$A_{ab}^\dagger(JM) = \mathcal{N}_{ab}^J \sum_{m_a m_b} C_{j_a m_a j_b m_b}^{JM} \alpha_{a m_a}^\dagger \alpha_{b m_b}^\dagger, \quad (\text{B3})$$

$$B_{ab(J_s)v}^\dagger(JM) = \sum_{M_s \mu} C_{J_s M_s \lambda \mu}^{JM} A_{ab}^\dagger(J_s M_s) Q_{v \lambda \mu}^\dagger. \quad (\text{B4})$$

$Q_{v \lambda \mu}^\dagger$  is the phonon creation operator in the QRPA model,

$$Q_{v \lambda \mu}^\dagger = \sum_{ab} X_{ab}^{v \lambda} A_{ab}^\dagger(\lambda \mu) - (-)^{\lambda + \mu} Y_{ab}^{v \lambda} A_{ab}(\lambda - \mu). \quad (\text{B5})$$

The expressions of the QPVC matrix elements  $A^{(2)}$  are

$$A_{ab,a'b'(J_s)\nu}^{(2)J}(1) = \delta_{bb'} \mathcal{N}_{ab}^J \mathcal{N}_{a'b'}^{J_s} (-)^{j_a+j_{b'}+\lambda+J_s} \hat{f}_s \left\{ \begin{matrix} j_a' & j_{b'}' & J_s \\ J & \lambda' & j_a \end{matrix} \right\} \langle a||V||a'\nu \rangle; \quad (\text{B6a})$$

$$A_{ab,a'b'(J_s)\nu}^{(2)J}(2) = (-) \delta_{ab'} \mathcal{N}_{ab}^J \mathcal{N}_{a'b'}^{J_s} (-)^{j_b+j_{b'}+\lambda+J_s} \hat{f}_s \left\{ \begin{matrix} j_a' & j_{b'}' & J_s \\ J & \lambda & j_b \end{matrix} \right\} (-)^{j_a+j_b+J} \langle b||V||a'\nu \rangle; \quad (\text{B6b})$$

$$A_{ab,a'b'(J_s)\nu}^{(2)J}(3) = \delta_{aa'} \mathcal{N}_{ab}^J \mathcal{N}_{a'b'}^{J_s} (-)^{j_{a'}+j_{b'}+\lambda+J} \hat{f}_s \left\{ \begin{matrix} j_a' & j_{b'}' & J_s \\ \lambda & J & j_b \end{matrix} \right\} \langle b||V||b'\nu \rangle; \quad (\text{B6c})$$

$$A_{ab,a'b'(J_s)\nu}^{(2)J}(4) = (-) \delta_{ba'} \mathcal{N}_{ab}^J \mathcal{N}_{a'b'}^{J_s} (-)^{j_{a'}+j_{b'}+\lambda+J} \hat{f}_s \left\{ \begin{matrix} j_a' & j_{b'}' & J_s \\ \lambda & J & j_a \end{matrix} \right\} (-)^{j_a+j_b+J} \langle a||V||b'\nu \rangle. \quad (\text{B6d})$$

$A^{(3)}$  can be easily obtained by the following relation,

$$A_{a'b'(J_s)\nu,ab}^{(3)J}(k) = [A_{ab,a'b'(J_s)\nu}^{(2)J}(k)]^*, \quad k = 1, 2, 3, 4 \quad (\text{B7})$$

where  $\langle a||V||b\nu \rangle$  is the QPVC vertex. Because the QPVC matrix elements  $A^{(2)}$  and  $A^{(3)}$  are independent from the magnetic quantum number  $M$ , we omit it throughout the paper.

For diagrams E, E', F, and F', the QPVC matrix elements  $A_{a_2b_2(\lambda)N_f,a_1b_1}^{(3)J_i}(1)$ ,  $A_{a_2b_2(\lambda)N_f,a_1b_1}^{(3)J_i}(2)$ ,  $A_{a_2b_2(\lambda)N_f,a_1b_1}^{(3)J_i}(3)$ , and  $A_{a_2b_2(\lambda)N_f,a_1b_1}^{(3)J_i}(4)$  are involved. For diagrams G, G', H, and H', the QPVC matrix elements  $A_{a_2b_2,a_1b_1(J_f)N_i}^{(2)\lambda}(1)$ ,  $A_{a_2b_2,a_1b_1(J_f)N_i}^{(2)\lambda}(2)$ ,  $A_{a_2b_2,a_1b_1(J_f)N_i}^{(2)\lambda}(3)$ , and  $A_{a_2b_2,a_1b_1(J_f)N_i}^{(2)\lambda}(4)$  are involved. For diagrams I, I', J, and J', the QPVC matrix elements  $A_{a_2b_2,a_1b_1(\lambda)N_i}^{(2)J_f}(1)$ ,  $A_{a_2b_2,a_1b_1(\lambda)N_i}^{(2)J_f}(2)$ ,  $A_{a_2b_2,a_1b_1(\lambda)N_i}^{(2)J_f}(3)$ , and  $A_{a_2b_2,a_1b_1(\lambda)N_i}^{(2)J_f}(4)$  are involved. For diagrams K, K', L, and L', the QPVC matrix elements  $A_{a_2b_2(J_i)N_f,a_1b_1}^{(3)\lambda}(1)$ ,  $A_{a_2b_2(J_i)N_f,a_1b_1}^{(3)\lambda}(2)$ ,  $A_{a_2b_2(J_i)N_f,a_1b_1}^{(3)\lambda}(3)$ , and  $A_{a_2b_2(J_i)N_f,a_1b_1}^{(3)\lambda}(4)$  are involved.

### Appendix C: QPVC and QRPA vertices

The QPVC vertex is evaluated as [39, 52]

$$\begin{aligned} \langle a||V||a'\nu \rangle = & \hat{\lambda}' \mathcal{N}_{aa'}^{\lambda'-1} \sum_{a_0b_0} X_{a_0b_0}^{v'\lambda'} [(v_a^* v_{a'} v_{a_0} u_{b_0} - u_a^* u_{a'} u_{a_0} v_{b_0}) \langle [a(a')^{-1}]_{\lambda'} | V | [a_0(b_0)^{-1}]_{\lambda'} \rangle \\ & + (-)^{j_{a_0}+j_{b_0}+\lambda'} (u_a^* u_{a'} v_{a_0} u_{b_0} - v_a^* v_{a'} u_{a_0} v_{b_0}) \langle [a(a')^{-1}]_{\lambda'} | V | [b_0(a_0)^{-1}]_{\lambda'} \rangle \\ & - (v_a^* u_{a'} v_{a_0} v_{b_0} - u_a^* v_{a'} u_{a_0} u_{b_0}) \langle (aa')_{\lambda'} | V | (a_0b_0)_{\lambda'} \rangle] \\ & - (-)^{j_a+j_{a'}+\lambda'} Y_{a_0b_0}^{v'\lambda'} [(v_{a'} v_a^* u_{a_0}^* u_{b_0}^* - u_{a'}^* u_a^* u_{a_0}^* v_{b_0}^*) \langle [a'(a)^{-1}]_{\lambda'} | V | [a_0(b_0)^{-1}]_{\lambda'} \rangle \\ & + (-)^{j_{a_0}+j_{b_0}+\lambda'} (u_{a'}^* u_a^* v_{a_0}^* u_{b_0}^* - v_{a'}^* v_a^* u_{a_0}^* v_{b_0}^*) \langle [a'(a)^{-1}]_{\lambda'} | V | [b_0(a_0)^{-1}]_{\lambda'} \rangle \\ & - (v_{a'} u_a^* v_{a_0}^* v_{b_0}^* - u_{a'}^* v_a u_{a_0}^* u_{b_0}^*) \langle (a'a)_{\lambda'} | V | (a_0b_0)_{\lambda'} \rangle], \end{aligned} \quad (\text{C1})$$

with the coupled two-body interaction matrix elements

$$\langle a(a')^{-1}; \lambda' | V | a_0(b_0)^{-1}; \lambda' \rangle = \mathcal{N}_{aa'}^{\lambda'} \mathcal{N}_{a_0b_0}^{\lambda'} \sum_{m_a m_{a'} m_{a_0} m_{b_0}} (-)^{j_{a'}-m_{a'}+j_{b_0}-m_{b_0}} C_{j_a m_a j_{a'}-m_{a'}}^{\lambda' \mu'} C_{j_{a_0} m_{a_0} j_{b_0}-m_{b_0}}^{\lambda' \mu'} \bar{v}_{ab_0 a' a_0}, \quad (\text{C2})$$

$$\langle aa'; \lambda' | V | a_0 b_0; \lambda' \rangle = \mathcal{N}_{aa'}^{\lambda'} \mathcal{N}_{a_0 b_0}^{\lambda'} \sum_{m_a m_{a'} m_{a_0} m_{b_0}} C_{j_a m_a j_{a'} m_{a'}}^{\lambda' \mu'} C_{j_{a_0} m_{a_0} j_{b_0} m_{b_0}}^{\lambda' \mu'} \bar{v}_{aa' a_0 b_0}. \quad (\text{C3})$$

The QRPA vertices  $\langle \nu || V || ab \rangle$  and  $\langle ab, \nu || V || 0 \rangle$  can be easily evaluated by  $X_{ab}^{v\lambda}$  and  $Y_{ab}^{v\lambda}$  in the QRPA model,

$$\langle \nu || V || ab \rangle = \hat{\lambda} [\Omega_\nu - (E_a + E_b)] X_{ab}^{v\lambda}, \quad (\text{C4})$$

$$\langle ab, \nu || V || 0 \rangle = -\hat{\lambda} [\Omega_\nu + (E_a + E_b)] Y_{ab}^{v\lambda}. \quad (\text{C5})$$

- 
- [1] K. Alder, A. Bohr, T. Huus, B. Mottelson, and A. Winther, *Rev. Mod. Phys.* **28**, 432 (1956).
- [2] T. Glasmacher, *Annual Review of Nuclear and Particle Science* **48**, 1 (1998).
- [3] D. Cline, *Ann. Rev. Nucl. Part. Sci.* **36**, 683 (1986).
- [4] S. Raman, C. Nestor, and P. Tikkanen, *At. Data Nucl. Data Tables* **78**, 1 (2001).
- [5] R. Taniuchi, C. Santamaria, P. Doornenbal, and et al., *Nature* **569**, 53 (2019).
- [6] F. Camera, J. Isaak, A. Maj, and S. Siem, *Eur. Phys. J. A* **59**, 168 (2023).
- [7] G. F. Bertsch, P. F. Bortignon, and R. A. Broglia, *Rev. Mod. Phys.* **55**, 287 (1983).
- [8] J. R. Beene, F. E. Bertrand, M. L. Halbert, R. L. Auble, D. C. Hensley, D. J. Horen, R. L. Robinson, R. O. Sayer, and T. P. Sjoreen, *Phys. Rev. C* **39**, 1307 (1989).
- [9] J. R. Beene, F. E. Bertrand, D. J. Horen, R. L. Auble, B. L. Burks, J. Gomez del Campo, M. L. Halbert, R. O. Sayer, W. Mittig, Y. Schutz, J. Barrette, N. Alamanos, F. Auger, B. Fernandez, A. Gillibert, B. Haas, and J. P. Vivien, *Phys. Rev. C* **41**, 920 (1990).
- [10] J. Isaak, D. Savran, M. Krtićka, and et al., *Phys. Lett. B* **727**, 361 (2013).
- [11] B. Wasilewska, M. Kmiecik, M. Ciemafa, and et al., *Phys. Rev. C* **105**, 014310 (2022).
- [12] H. R. Weller, M. W. Ahmed, H. Gao, W. Tornow, Y. K. Wu, M. Gai, and R. Miskimen, *Prog. Part. Nucl. Phys.* **62**, 257 (2009).
- [13] J. Kleemann, N. Pietralla, U. Friman-Gayer, and et al., *Phys. Rev. Lett.* **134**, 022503 (2025).
- [14] O. Papst, J. Isaak, V. Werner, and et al., *Phys. Rev. Lett.* **135**, 052501 (2025).
- [15] A. Konig, S. Hilaire, and S. Goriely, *Eur. Phys. J. A* **59**, 131 (2023).
- [16] M. Ballan, S. Bottoni, M. Caamaño, and et al., *Eur. Phys. J. Plus* **138**, 709 (2023).
- [17] K.-J. Chen, L.-X. Liu, Z.-R. Hao, and et al., *Nucl. Sci. Tech.* **34**, 47 (2023).
- [18] P. F. Bortignon, R. A. Broglia, and G. F. Bertsch, *Phys. Lett. B* **148**, 20 (1984).
- [19] D. Bes, P. Curutchet, S. Reich, N. Scoccola, and H. Sofia, *Nucl. Phys. A* **452**, 531 (1986).
- [20] J. Speth, D. Cha, V. Klemt, and J. Wambach, *Phys. Rev. C* **31**, 2310 (1985).
- [21] V. Voronov and V. Ponomarev, *Nucl. Phys. A* **520**, c619 (1990), nuclear Structure in the Nineties.
- [22] V. Ponomarev and A. Krasznahorkay, *Nucl. Phys. A* **550**, 150 (1992).
- [23] M. Brenna, G. Colò, and P. F. Bortignon, *Phys. Rev. C* **85**, 014305 (2012).
- [24] W. L. Lv, Y. F. Niu, and G. Colò, *Phys. Rev. C* **103**, 064321 (2021).
- [25] E. Litvinova and P. Ring, *Phys. Rev. C* **73**, 044328 (2006).
- [26] G. Colò, H. Sagawa, and P. F. Bortignon, *Phys. Rev. C* **82**, 064307 (2010).
- [27] E. V. Litvinova and A. V. Afanasjev, *Phys. Rev. C* **84**, 014305 (2011).
- [28] G. Colò, P. F. Bortignon, and G. Bocchi, *Phys. Rev. C* **95**, 034303 (2017).
- [29] Y. F. Niu, G. Colò, and E. Vigezzi, *Phys. Rev. C* **90**, 054328 (2014).
- [30] Y. F. Niu, Z. M. Niu, G. Colò, and E. Vigezzi, *Phys. Rev. Lett.* **114**, 142501 (2015).
- [31] Y. Niu, Z. Niu, Colò, and E. Vigezzi, *Phys. Lett. B* **780**, 325 (2018).
- [32] C. Robin and E. Litvinova, *Phys. Rev. Lett.* **123**, 202501 (2019).
- [33] E. Litvinova, C. Robin, and H. Wibowo, *Phys. Lett. B* **800**, 135134 (2020).
- [34] Q. Liu, J. Engel, N. Hinohara, and M. Kortelainen, *Phys. Rev. C* **109**, 044308 (2024).
- [35] X. Roca-Maza, Y. F. Niu, G. Colò, and P. F. Bortignon, *J. Phys. G: Nucl. Part. Phys.* **44**, 044001 (2017).
- [36] S. Shen, G. Colò, and X. Roca-Maza, *Phys. Rev. C* **101**, 044316 (2020).
- [37] Z. Z. Li, Y. F. Niu, and G. Colò, *Phys. Rev. Lett.* **131**, 082501 (2023).
- [38] E. Litvinova, *Phys. Rev. C* **107**, L041302 (2023).
- [39] Z. Z. Li, Y. F. Niu, and G. Colò, *Phys. Rev. C* **110**, 064317 (2024).
- [40] J. Kleemann, *Probing the Giant Dipole Resonance Using Nuclear Resonance Fluorescence*, *Ph.D. thesis* (2024).
- [41] B. Mottelson, *Rev. Mod. Phys.* **48**, 375 (1976).
- [42] P. Bortignon, R. Broglia, D. Bes, and R. Liotta, *Phys. Rep.* **30**, 305 (1977).
- [43] A. Bohr and B. R. Mottelson, *Nuclear Structure*, 2nd ed., Vol. I (W. A. Benjamin Inc., New York, 1998) p. 388.
- [44] A. Bohr and B. R. Mottelson, *Nuclear Structure*, 2nd ed., Vol. II (W. A. Benjamin Inc., New York, 1998) p. 486.
- [45] A. Leprêtre, H. Beil, R. Bergère, and et al., *Nucl. Phys. A* **258**, 350 (1976).
- [46] L. Peker, *Nucl. Data Sheets* **73**, 261 (1994).
- [47] M. Beiner, H. Flocard, N. V. Giai, and P. Quentin, *Nucl. Phys. A* **238**, 29 (1975).
- [48] N. V. Giai and H. Sagawa, *Phys. Lett. B* **106**, 379 (1981).
- [49] J. Bartel, P. Quentin, M. Brack, C. Guet, and H.-B. Håkansson, *Nucl. Phys. A* **386**, 79 (1982).
- [50] L. G. Cao, U. Lombardo, C. W. Shen, and N. V. Giai, *Phys. Rev. C* **73**, 014313 (2006).
- [51] J. Suhonen, *From Nucleons to Nucleus*, Theoretical and Mathematical Physics (Springer Berlin, Heidelberg, 2007).
- [52] Y. F. Niu, G. Colò, E. Vigezzi, C. L. Bai, and H. Sagawa, *Phys. Rev. C* **94**, 064328 (2016).